ACS APPLIED ELECTRONIC MATERIALS

pubs.acs.org/acsaelm Article

Self-Powered Sterilization System for Wearable Devices Based on Biocompatible Materials and Triboelectric Nanogenerator

Danni Lei,[⊥] Junpeng Wu,[⊥] Yunlong Zi, Caofeng Pan,* Hongzhi Cui,* and Xiaoyi Li*

Cite This: *ACS Appl. Electron. Mater.* 2023, 5, 2819−2828 Read Online

ACCESS | Metrics & More | Article Recommendations | Supporting Information

ABSTRACT: Wearable electronics with multifunction and convenience are entering a period of rapid development. However, the longer people wear electronic devices, the easier it is for bacteria to infect the skin. Sterilization of wearables has received little research, partly because mature high-voltage sterilization systems require energy sources, which will greatly restrict the large-scale applications of wearable devices. Therefore, a self-powered sterilization system with high comfort and safety is strongly appealing. To solve the above problem, we design a wearable, self-powered sterilization system with a biocompatible nano/microporous fiber triboelectric nanogenerator (NMF-TENG) as the energy source and an interdigital electrode for better bactericidal performance. Ag nanowires (AgNWs) and carbon nanotube (CNT) are added to the indium tin oxide (ITO)-based interdigital electrode to improve the conductivity, bending performance, and local electric field strength. Due to the tip effect, the local electric field of the electrode can be improved as high as 1 MV m^{-1}, which can kill the bacteria. The system can achieve a long-term sterilization rate of up to 90%, which has great application potential in the sterilization direction of wearable electronic devices.

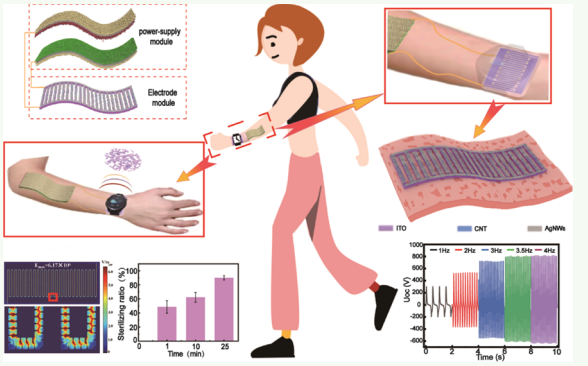

KEYWORDS: *sterilizations, self-powered, triboelectric nanogenerator, AgNWs/CNT nanowires, biocompatible materials*

1. INTRODUCTION

Integrated circuits are becoming increasingly sophisticated with the advent of big data information.[1−4] Humans are entering the wearable electronics era, and a variety of small wearable electronics are ushering in a near "blowout" development.[5−7] Although most wearable electronics were in direct contact with skin,[8] as wear time increases, there is an increasing amount of bacteria and microorganisms between electronic devices and the skin, which becomes a huge potential hazard to healthy living.[9] The use of wearable electronic devices with antibacterial[10] or bactericidal functions[11,12] is attracting increasing attention. There has been a great deal of research on antibacterial functions. For example, Alizadeh et al.[13] successfully loaded different concentrations of meropenem and colistin antibiotics into chitosan/poly(vinyl alcohol) (CS/PVA) electrospinning pads to fabricate wound dressings with excellent antibacterial properties. But the overuse of antibiotics has made the bacteria increasingly resistant, making it difficult to develop appropriate drugs to remove them quickly.[14]

High-voltage sterilization technology (HVST) is an effective bactericidal method that relies on a strong electric field to damage the external structure of the microbes (bacterial membranes and viral capsids) and thus destroy biological activity.[15−17] Nanowires (such as Ag, CuO, and ZnO nanowires) have been used to generate locally enhanced electric fields under both direct current and alternating current conditions.[18−20] However, they are effective and practical demonstrating strong dependence on the external power source, which will greatly restrict the large-scale applications of wearable devices. Therefore a self-powered sterilization system is strongly appealing. The triboelectric nanogenerator (TENG), which harvests low-frequency and disordered energy, is compatible as a power module in various complex environments.[21−29] The TENG can realize high-voltage and low-current output characteristics without complicated circuitry, which improves safety while achieving the sterilization process and perfectly fulfills the sterilization requirements of wearable electronics.[30−40] Unfortunately, the output of most wearable TENGs currently under investigation is only a few to tens or hundreds of volts,[41−45] which is not sufficient to generate a local electric field for sterilization of the local electric field intensity needed to exceed 10^6 V m^{-1} to achieve effective sterilization.[46−49]

Received: February 28, 2023
Accepted: April 26, 2023
Published: May 5, 2023

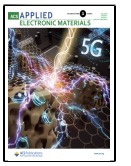

https://doi.org/10.1021/acsaelm.3c00262
ACS Appl. Electron. Mater. 2023, 5, 2819−2828

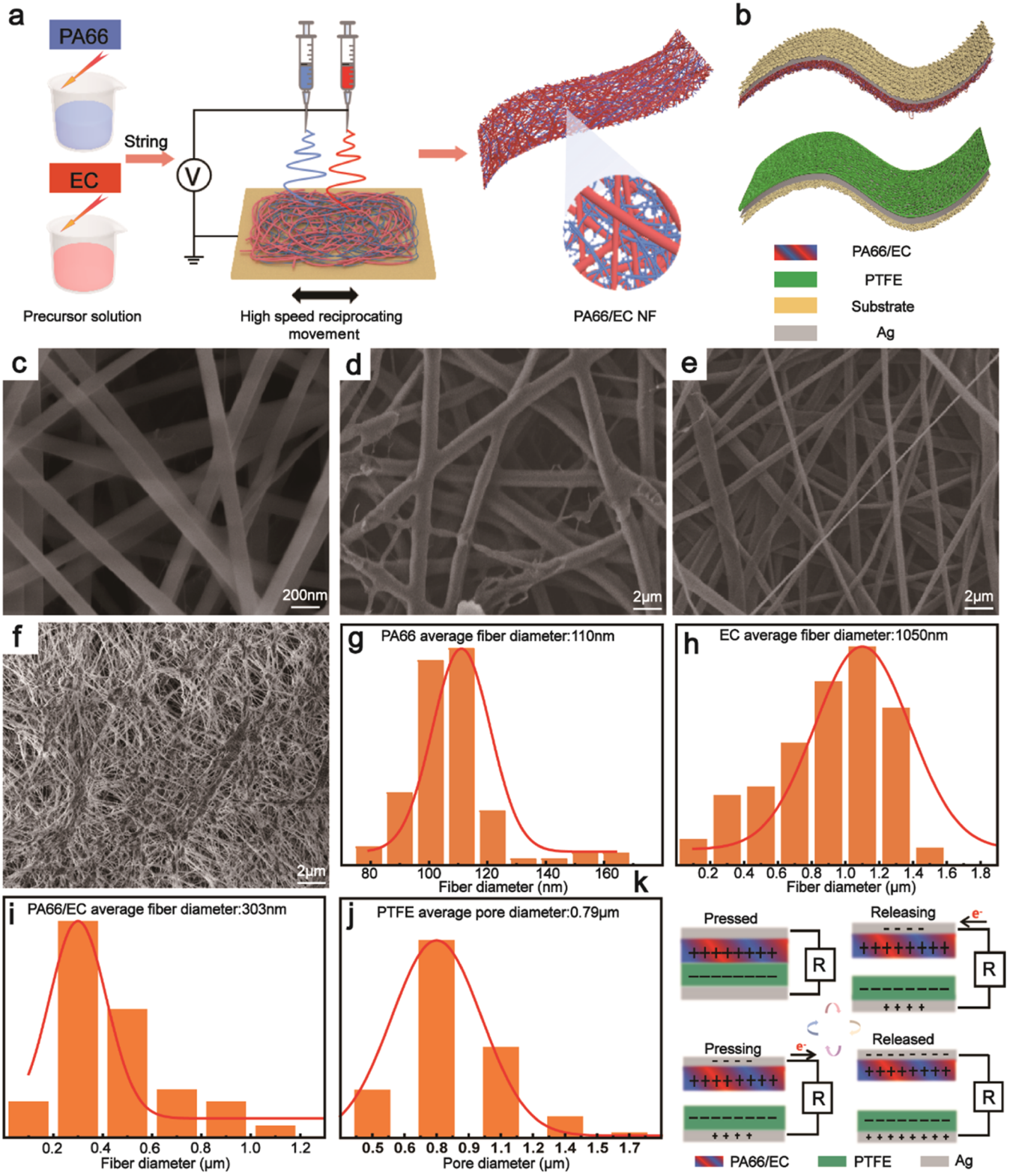

Figure 1. Schematic diagrams of the nano/microporous-fibrous-based triboelectric nanogenerator (NMF-TENG). (a) Illustration of fabrication processing of PA66/EC nanofibers films; (b) simulation diagram: (c–f) SEM images of (c) PA66 nanofiber, (d) EC nanofiber, (e) PA66/EC nanofiber film, and (f) PTFE microporous film. (g–i) Diameter distributions of the electrospun fibers: (g) PA66, (h) EC, and (i) PA66/EC. (j) Pore diameter distribution of PTFE microporous membrane. (k) Schematic diagram of the working principle of the NMF-TENG during different states.

In this study, we designed a wearable, self-powered sterilization system, which used the biocompatible nano/microporous fiber triboelectric nanogenerator (NMF-TENG) as the energy source and an interdigital electrode for better bactericidal performances. Industrial microporous poly(tetrafluoroethylene) (PTFE) film and PA66/ethyl cellulose

https://doi.org/10.1021/acsaelm.3c00262
ACS Appl. Electron. Mater. 2023, 5, 2819–2828

(EC) nanofiber composite film were used as the friction layer to ensure the electrical output and flexibility of the NMF-TENG. The PA66/EC nanofiber composite films were prepared by electrospinning, and the optimum parameters of PA66/EC composite fiber films with different mass ratios were systematically studied to improve the electrical output of TENG further. The NMF-TENG could achieve a stable output of 302 V and 0.4 μA at a low frequency of 1 Hz, which meets the power supply requirements of sterilization systems. Ag nanowires (AgNWs) and carbon nanotubes (CNTs) were added to the indium tin oxide (ITO) to improve the conductivity, bending performance, and local electric field strength. Then, AgNWs/CNT/ITO nanowire flexible interdigital electrodes were prepared by spin coating and direct laser writing. Due to the tip effect, the local electric field of the electrode could be improved as high as 1 MV m^{-1}, which could kill the bacteria effectively. Meanwhile, the high electric field between the composited electrodes may further enhance the effect of antibacterial ion Ag^+ in AgNWs, further improving the bactericidal effect. Finally, the self-powered sterilization system had a sterilization rate of about 90% after 25 min of operation with the NMF-TENG, which showed great application potential in the direction of wearable electronic sterilization. This study would significantly improve our understanding of the working principle of the bactericidal process and promote the commercialization of TENG-based self-powered sterilization systems in the future.

2. EXPERIMENTAL SECTION

2.1. Electrospinning of PA66/EC Nanofibers Films. *2.1.1. Preparation of Electrospinning Precursor.* The EC powder was dissolved in 10 wt % absolute ethanol solvent at room temperature by continuous magnetic stirring for 12 h. At the same time, a certain amount of PA66 particles was accurately weighed and dissolved in formic acid solution for 12 h by magnetic stirring to obtain PA66 solution (18 wt %).

The PA66 and EC spinning solution needles at the ratio of 10/0, 7/3, 6/4, 5/5, 4/6, and 3/7 were multineedle electrospun at a spinning voltage of 18 kV and a receiving distance of 15 cm (the moving speed of the high-speed reciprocating device is 0.1 m s^{-1}). Nozzles with an inner diameter of 0.6 mm were used for spinning, and the sample injection speed was 0.5 mL h^{-1}. The PA66/EC composite nanofiber films are collected on a flexible PTFE substrate coated with a conductive silver layer at a temperature of 25 ± 2 °C and a relative humidity of 30 ± 2%. The surface morphologies of PA66 film, EC film, PA66/EC film, and PTFE film were characterized by field emission scanning electron microscopy (SEM).

2.2. Assembly of NMF-TENG. PA66/EC nanofiber membranes with different mass ratios were used as the positive-friction materials of NMF-TENG. Then, a PTFE microporous film (aperture: 0.45 μm) and PTFE substrate (Guangzhou CleverFlon New Materials Technology Co., LTD) sprayed with the conductive silver layer were bonded together as the friction electrode layer. In addition, PA66/EC nanofiber membrane and PTFE microporous membrane were cut into squares of dimensions 6 cm × 6 cm. The two friction materials were assembled into a triboelectric nanogenerator with a vertical separation structure through an external wire. The electrical output signals of TENGs were examined using an electrometer (Keithley 6514).

2.3. Fabrication of AgNWs/CNT/ITO Nanowire Interdigital Electrodes. A proper amount of carbon nanotube CNT (*N*-methylpyrrolidone(NMP)) (Aladdin) slurry was dropped onto the flexible ITO/fluorinated ethylene propylene (FEP) film substrate, and a conductive hydrophilic coating of carbon nanotube with uniform thickness was obtained by high-speed spin coating. Then, an appropriate amount of AgNWs ethanol dispersion was spun onto the CNT-ITO substrate and AgNWs/CNT/ITO films were obtained after solvent volatilization. Subsequently, AgNWs/CNT/ITO laser scribing was performed using a G·WEIKE laser system under environmental conditions. Here, the optimized laser power of 12 W with a scanning speed of 80 mm s^{-1} was chosen based on the balance between production efficiency and production stability. To obtain AgNWs/CNT/ITO nanowire interdigital electrode films with certain patterns, interdigital electrodes of the same size without nanowires were prepared similarly.

2.4. Assembly of Wearable Self-Powered Long-Acting Germicide Device. The ends of the AgNWs/CNT/ITO nanowire interdigital electrodes were connected to the two terminals of NMF-TENG with wires. Comsol simulation was performed on the electric field distribution of single-pair electrodes, interdigital electrodes without nanowire modification, and interdigital electrodes modified by nanowires.

2.5. Antibacterial Performance of Wearable Self-Powered Long-Acting Germicide Device. *Escherichia coli* were cultured to measure the antibacterial properties of AgNWs/CNT/ITO nanowire interdigital electrodes with the NMF-TENG system. The fresh bacterial suspension was acquired by culturing *E. coli* in a sterile LB medium at 37 °C for 24 h. Subsequently, the concentration of bacterial suspension was measured using the spread plate method and then diluted using sterilized phosphate-buffered saline (PBS) to get an initial culture concentration of colony-forming units of ∼10^6 CFU mL^{-1}. 500 μL of *E. coli* solution was inoculated on FEP, AgNWs/CNT nanowire interdigital electrodes were covered on the thin film, encapsulated NMF-TENG and AgNWs/CNT nanowire interdigital electrodes are connected with microwires, and electrically stimulated films of different times were incubated in Petri dishes for 24 h. The number of live bacteria growing on different samples after 24 h of incubation was counted with image software measurement. The number of bacteria in the original group was denoted by *A*, and that in the treated sample was denoted by *B*. Finally, the bacterial survival rate (R) was calculated by formula 1

$$\text{bacterial survival ratio } (R) = 1 - (A - B/A \times 100\%) \quad (1)$$

3. RESULTS AND DISCUSSION

3.1. Surface Morphologies of Friction Materials. A schematic of the PA66/EC nanofiber membrane electrospinning process is presented in Figure 1a and detailed in the experimental part. The structure of NMF-TENG is shown in Figure 1b, in which the PA66/EC nanofiber film and the microporous PTFE film acted as a friction layer for contact electrification, and a layer of silver sprayed on a substrate was used for charge transmission. The microscopic morphology of the pure PA66 nanofiber film and the pure EC nanofiber film is shown in Figure 1c,d. It should be noted that the spinning conditions described above optimized the experimental results. We could find from the SEM image that pure PA66 film nanofibers (Figure 1c) have smooth surface and appreciable diameter and are evenly distributed. The mean diameter of its fibers (Figure 1g) was only 110 nm, and thus PA66 showed an excellent spin-casting performance. Under the same conditions, however, the fiber diameter of the pure EC movie (Figure 1d) was uneven. The fiber's surface was rough, and thus severe sticking took place. At the same time, the average EC fiber diameter (1050 nm) shown in Figure 1h was much larger than that of the PA66 fiber. This is mainly due to the very high viscosity of the EC spinning solution, and the tensile force generated by the high-pressure electric field on the solution jet is unstable, leading to the poor electrostatic spinnability of EC, which is not conducive to the production of continuous and stable high triboelectric output (Figure S1).

For this reason, PA66 was used as a member of two-component co-electrostatic EC spinning to improve EC

https://doi.org/10.1021/acsaelm.3c00262
ACS Appl. Electron. Mater. 2023, 5, 2819−2828

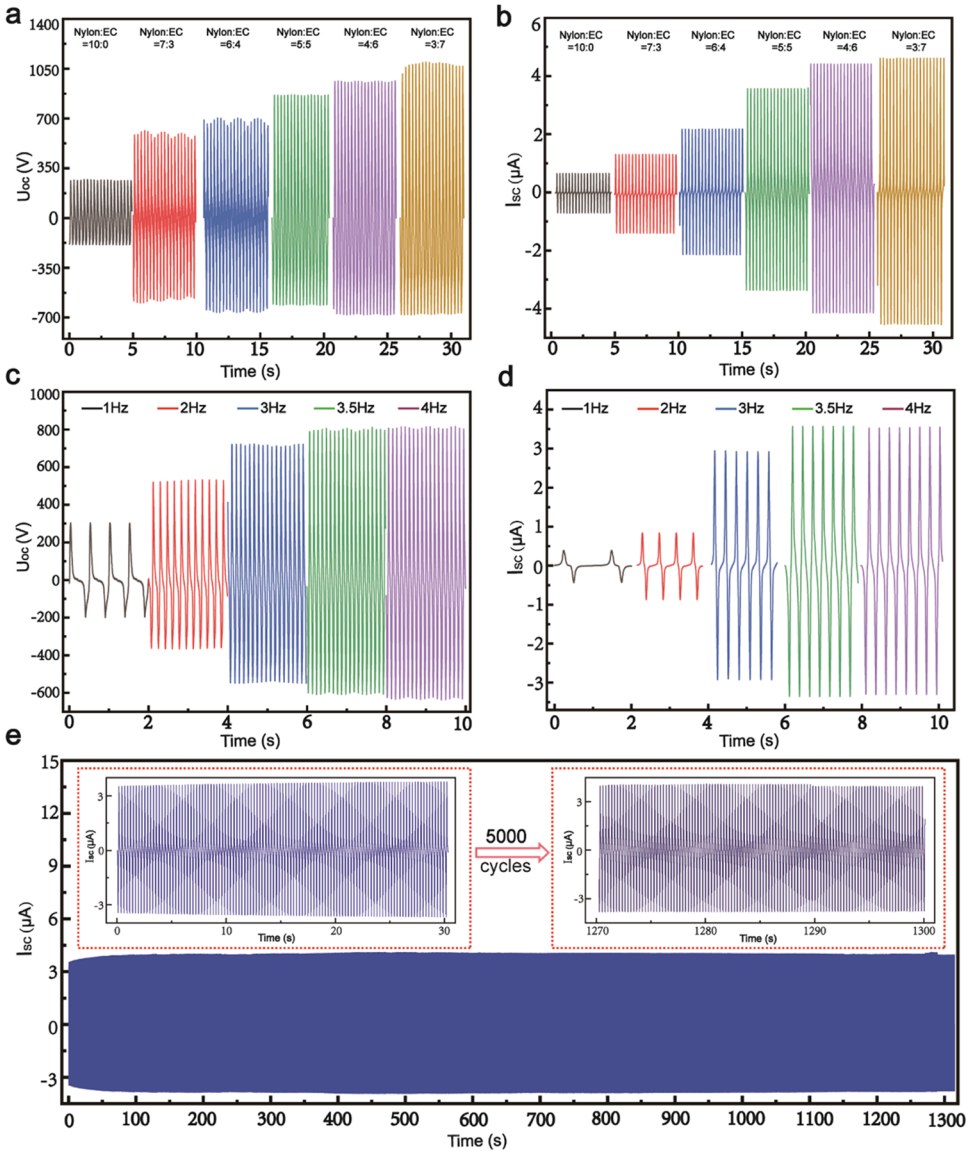

Figure 2. Output performance of NMF-TENG. (a, b) Open-circuit voltage (V_{oc}) and short-circuit current (I_{sc}) of NMF-TENGs constructed from PA66/EC nanofiber membranes with different mass ratios. (c, d) V and I_{sc} of NMF-TENGs under different impact frequencies at PA66 and EC at the best quality (PA66/EC = 5:5). (e) Mechanical durability characterization with 5000 continuous working cycles.

spinning performance. As can be seen in Figure 1e, at the ratio of PA66/EC = 5:5, the PA66/EC fiber was straight and smooth, and thus had good flexibility, which was also convenient for the NMF-TENG to form a reliable device structure and therefore generated a stable, high triboelectric power output. At the same time, adding PA66 reduced the diameter distribution range of the PA66/EC fibers (Figure 1i), ranging between 100 and 900 nm, with a mean diameter of 303 nm. Furthermore, porous PTFE fiber films (Figure 1f) had a prominent pore structure and a three-dimensional mesh structure, and the average pore size (Figure 1j) was approximately 0.8 μm in size. In addition to increasing the surface roughness, the PA66/EC and PTFE nanomesh structure also improved the specific surface area.

In comparison, the presence of EC induced a higher surface charge density. This cooperative effect had the potential to significantly improve the electrical performance of the NMF-TENG while providing wearable comfort. The detailed mechanism of the NMF-TENG is graphically described in Figure 1k. The triboelectrification process occurred when the triboelectric material was in close contact. The different triboelectric polarities at the surface of the two triboelectric materials would generate positive and negative charges on the surface, respectively. At the time of separation, there is a difference in electrical potential between the two. Electrostatic induction would cause free electrons to be transferred from the lower electrode to the upper electrode by an external load, resulting in a displacement current. When the two were completely separated, their potential difference reached its maximum, resulting in a temporary equilibrium of the potential. In this case, the re-contact process would break the initial potential equilibrium, causing electrons from the PA66/EC film to flow back into the PTFE film. The potential difference became zero when both sides were in full contact. Repeated contact and separation convert mechanical energy into a continuous pulse of alternating electrical signals.

3.2. Electrical Output Performance of the NMF-TENG.

PA66/EC films with different mass ratios were assembled with

https://doi.org/10.1021/acsaelm.3c00262
ACS Appl. Electron. Mater. 2023, 5, 2819−2828

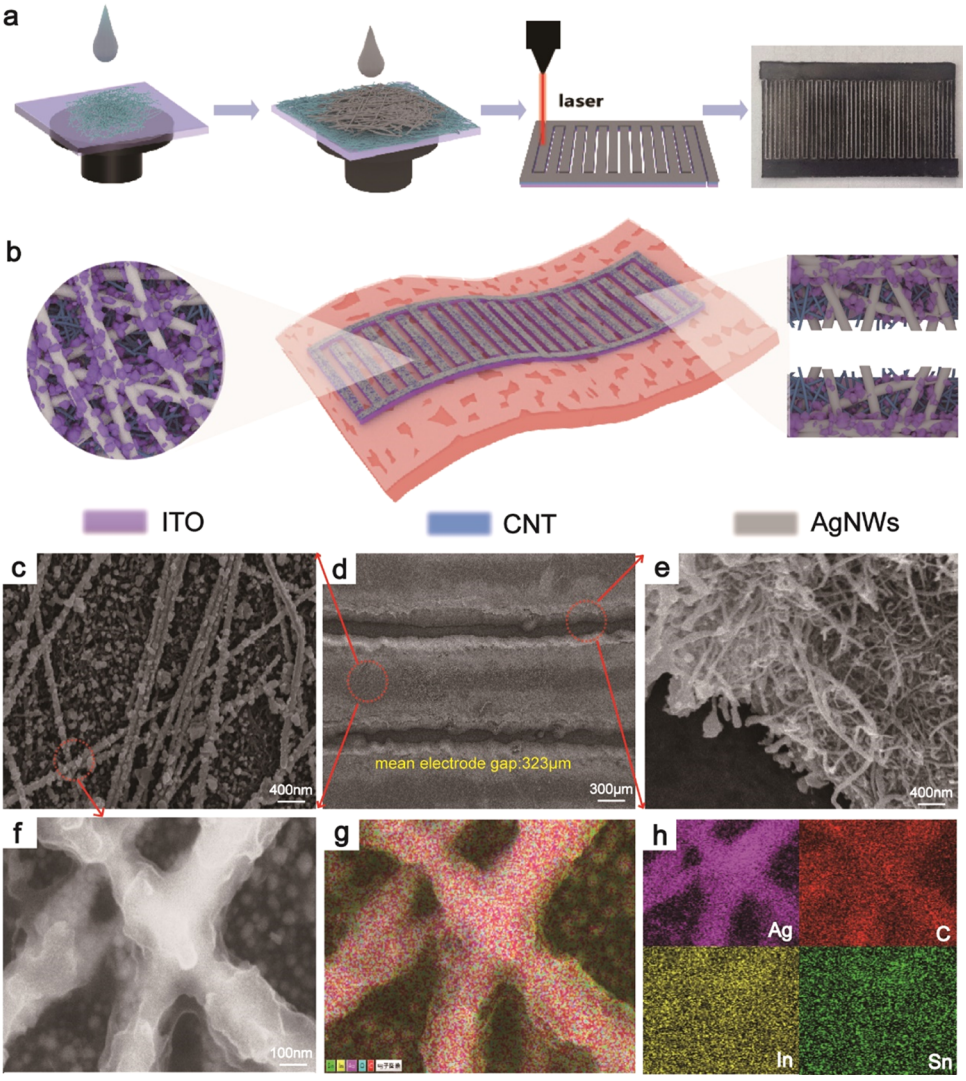

Figure 3. Fabrication and characterization of laser-scribed AgNWs/CNT/ITO nanowire interdigital electrode. (a) Illustration of the manufacturing process of AgNWs/CNT/IT nanowire interdigital electrode. (b) Schematic of the AgNWs/CNT/ITO nanowire interdigital electrodes. SEM images of AgNWs/CNT/ITO nanowire interdigital electrodes surface: (c) scale bar, 400 nm; (d) scale bar, 300 μm. (e) Interdigital electrode gap of nanowires; scale bar, 400 nm. (f–h) EDS analysis of AgNWs/CNT/ITO nanowire interdigital electrodes.

microporous PTFE films, and the open-circuit voltage and short-circuit current were measured. As shown in Figure 2a,b, the electrical output performance of NMF-TENG was greatly improved with the increase of EC proportion. When PA66/EC = 3:7, the short-circuit current (I_{sc}) and open-circuit voltage (V_{oc}) were as high as 4.6 μA and 1080 V, respectively, corresponding to 7.6 and 4 times pure PA66 fiber film. While the high EC content improved the frictional positive bias capability of the material, numerous flat structures were observed in the nanocomposite thin-film fiber structure (Figure S2a) in the PA66/EC = 3:7 condition, which significantly reduced its mechanical strength for the TENG application. As shown in Figure S2, as the proportion of PA66 components increased, beads on the fiber gradually disappeared. In the case of the PA66/EC = 5:5 mass ratio (Figure S2c), the PA66/EC fibers exhibited relatively uniform diameter distribution, and they were straight and smooth, thus exhibiting good flexibility, which was conducive to the formation of a reliable device structure and the generation of the stable high triboelectric output of NMF-TENG. When the ratio of PA66/EC = 5:5 was used, the electrical power was 3.5 μA and 866 V, which were 5.8 and 3.3 times those of the pure PA66 film, respectively.

Interestingly, after PA66/EC = 5:5, the relative increase in the output performance of NMF-TENG decreases, but the mechanical strength of the PA66/EC nanofiber films decreases even more. For this reason, the triboelectric properties of NMF-TENG at different contact frequencies were investigated by choosing PA66/EC = 5:5 nanofiber thin film as an optimized positive-friction material. Even at a frequency of 1 Hz, as shown in Figure 2c,d, the NMF-TENG could produce a high-voltage output of 302 V, ensuring strong power supply for a wearable self-propelled sterilizing device. When the frequency increases from 1 to 4 Hz, I_{sc} and V_{oc} increase from 0.4 μA and 308 V to 3.5 μA and 802 V, respectively, by 8.75 and 2.6 times. After the contact frequency was above 3.5 Hz, both I_{sc} and V_{oc} were approximately stable. This is because at high frequencies, since the accumulated surface charges could not be effectively canceled, this improved the rate of friction charge transfer. The outer electrons flow quickly to form an equilibrium state, thereby increasing the peak output. As the contact frequency was raised high enough, the

https://doi.org/10.1021/acsaelm.3c00262
ACS Appl. Electron. Mater. 2023, 5, 2819−2828

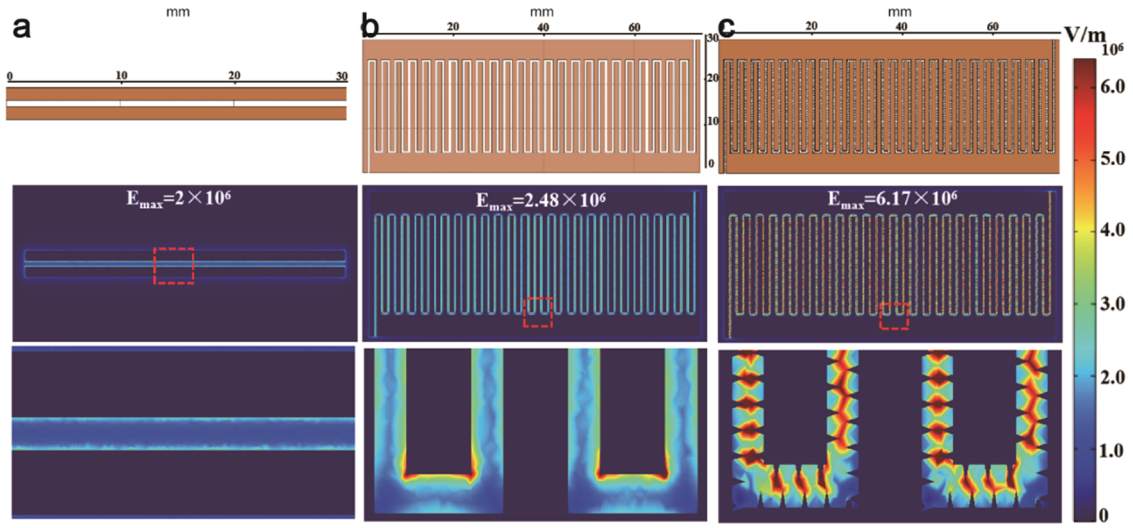

Figure 4. Electric field strength distribution for different electrode types at 200 V: (a) common electrode, (b) interdigital electrode (IE), (c) IE with AgNWs/CNT.

accumulated surface charge matched the transmission speed, so the output spike tended to be steady. The output stability of NMF-TENG was also investigated. The excellent output durability of the NMF-TENG was demonstrated by the stable triboelectric performance under 5000 consecutive periodic contact separation motions at a contact frequency of 3.5 Hz, as shown in Figure 2e, which shows the device's performance. In particular, the surface morphology of tribopositive PA66/EC nanofiber films maintained favorable structural integrity without obvious fiber break or wear after rigorous testing (Figure S3a,b), further demonstrating its potential in reality. The output voltage and current of the NMF-TENG were measured at 3.5 Hz using different resistances ranging from 1 kΩ to 1 GΩ resistor. As the external load was increased from 1 kΩ to 400 MΩ, the power density of the NMF-TENG was increased, reaching a peak power density load of 2.18 W m^{-2} of 400 MΩ (Figure S5). At the same time, in order to demonstrate the potential of high-performance frictional positive PA66/EC nanofiber film as a wearable power source, as shown in Figure S6, the assembled NMF-TENG is worn on the human body, which can generate enough electricity to drive the AgNWs/CNT/ITO nanowire interdigital electrode sterilization during human movement.

3.3. Surface Morphologies of AgNWs/CNT/ITO Nanowire Interdigital Electrodes. Figure 3a shows the preparation of patterned AgNWs/CNT/ITO nanowire interdigital electrodes using the laser writing technique. Briefly, CNTs dispersion of AgNWs was successfully coated onto the substrate surface of flexible ITO. In addition to acting as a conducting substance to increase conductivity, here CNT also acted as a hydrophilic coating to promote the adsorption of AgMWs. The patterned AgNWs/CNT/ITO nanowire flexible interdigital electrode was prepared by computer-controlled laser beam labeling after drying for 2 h at 60 °C in air. The preparation procedure is described in more detail in Section 2. The schematic diagram of AgNWs/CNT/ITO nanowire flexible interdigital electrodes prepared by laser etching is shown in Figure 3b. Since the prepared interdigital electrode had some flexibility, it could be fitted to the surface of human skin as a sterilizing electrode (Figure S7). The surface of the electrode was covered by a layer of complex three-dimensional AgNWs/CNT nanowire network structures. At the same time, laser writing also caused some ITO particles to spray onto the nanowires, giving the electrode good electrical conductivity. The AgNWs/CNT nanowires also caused a few nanoscale protrusions between the interstitial interdigitated electrodes. The tip discharge effect could be generated under NMF-TENG voltage, which could generate an electric field locally enhanced at the tip of the nanowire, reaching the intensity of cellular electroporation. This is also confirmed by the morphological characteristics of the electrode surface and the band gap collected by scanning electron microscopy (Figure 3c−e) that the AgNWs/CNT fiber network and the ITO nanoparticles are uniformly compounded together and that there were tiny protrusions of AgNWs/CNT nanowires at the edge of the electrode. AgNWs/CNT nanowires had a mean diameter of 19−85 nm (Figure S8), the mean width of the electrodes was 960 nm (Figure S9), the interelectrode gap was 323 nm (Figure S10), and there were microscopic protrusions of AgNWs/CNT nanosheets at the electrode edges. The composition of the AgNWs/CNT/ITO forked electrode elements was determined by EDX (Figure 3f,g). Elemental mapping (Figure 3h) of AgNWs/CNT/ITO showed the elemental dispersion of silver (Ag), carbon (C), indium (In), and tin (Sn), further confirming the successful loading of the AgNWs and CNT onto the ITO films.

To further prove that the nanowire interdigital electrode could locally increase the electric field, Comsol was used to simulate the electric field distribution of the single-pair electrode, the interdigital electrode without nanowire modification, and the interdigital electrode with nanowire modification. As the length of the gap of the interdigital electrode is much larger than traditional single-pair electrodes, there will be much more nanotips when the electrodes are covered by AgNWs/CNT. And these nanotips can provide much higher local electric field (Figure 4), thus improving the bactericidal performance. The simulation results (Figure 4a−c) showed that under the 200 V condition, increasing the logarithm of the electrodes has little effect on the electric field strength. On the other hand, modification of the AgNWs/CNT nanowires strongly enhances the electric field and the electric field intensity near the tip structure of the nanowires is

https://doi.org/10.1021/acsaelm.3c00262
ACS Appl. Electron. Mater. 2023, 5, 2819−2828

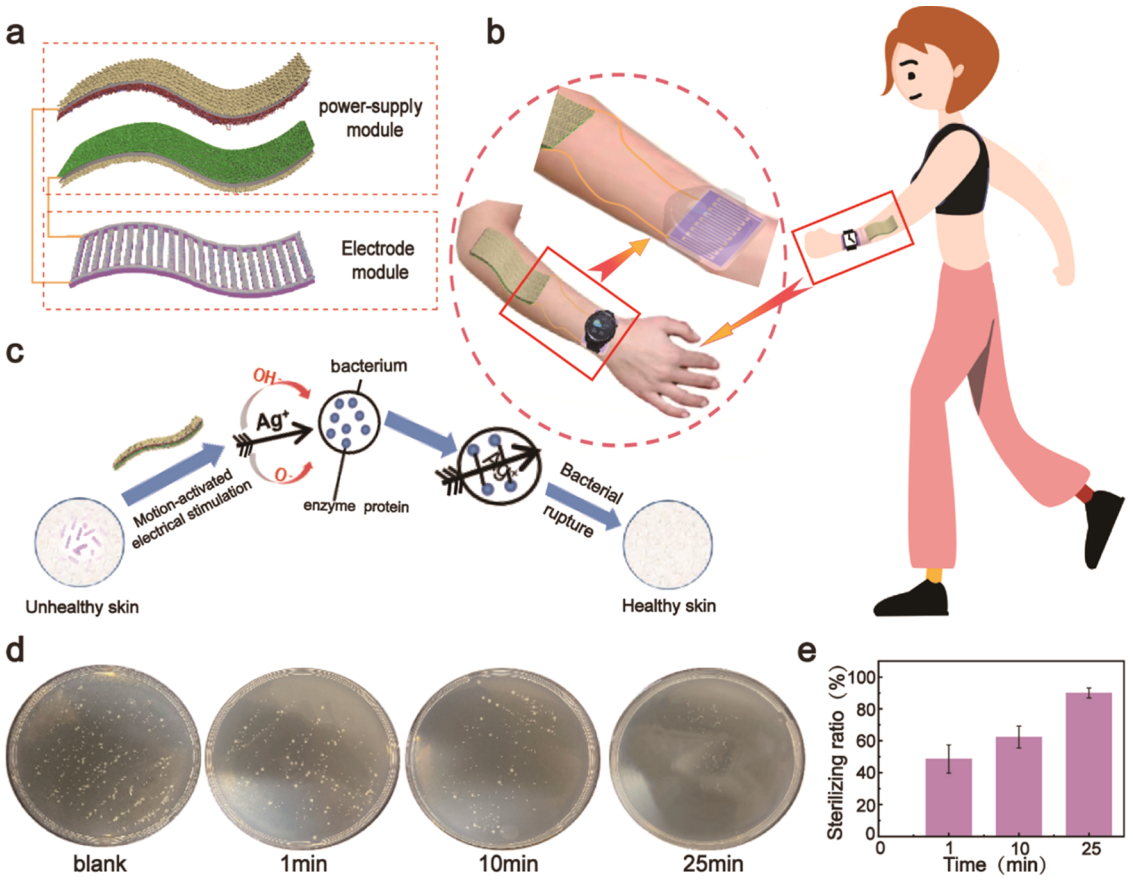

Figure 5. Schematic of motion-activated self-powered sterilization. (a) Constructional details of the wearable long-lasting sterilization devices, containing a power supply module NMF-TENG and AgNWs/CNT/ITO nanowires' flexible interdigital electrode. (b) Self-powered sterilization device worn on the human body; inset: self-powered power supply and AgNWs/CNT/ITO flexible interdigital electrode cooperate to effective sterilization. (c) Skin health restoration process of the wearable self-powered long-acting germicidal devices. (d) Image of viable bacteria grown after 24 h of culture on *E. coli* after different treatment times for wearable self-powered long-acting germicidal devices. (e) Disinfection efficiency of wearable self-powered long-acting germicidal devices on the *E. coli* under different processing times.

as high as 6.17 MV m^{-1}. The electric field intensity was increased by a factor of 2.48 compared to the interdigital electrode of the same size without modification of the nanowire. The literature has proved that once the electric field intensity reaches the critical value of 10^6 V m^{-1}, the strong electric field will destroy the cell membrane potential balance and kill bacteria. The stronger the electric field intensity, the more obvious the bactericidal effect. Therefore, the locally enhanced germicidal electric field generated by ITO flexible interdigital electrode modified by AgNWs/CNT has a stronger germicidal effect.

3.4. Wearable Long-Lasting Sterilization Device. To this end, a wearable self-powered stimulating nanowire interdigital electrode sterilization device was developed. The self-powered sterilization system for electrical stimulation consisted of one power module and one electrode module, as shown in Figure 5a. The battery module consisted of NMF-TENG, which was assembled in layers. The contact separation between micro- and nanoporous structures intersecting fiber films could convert low-frequency mechanical motion into electric energy to generate adjustable electric field intensity. The electrode module comprised AgNWs/CNT/ITO nanowire interdigital electrodes, which were integrated into the battery module through external leads (Figure S11), respectively. Both NMF-TENG and AgNWs/CNT/ITO interdigital electrodes had good wearing comfort and could realize wearable sterilization through simple circuit connection (Figure 5b). Then, we compared AgNWs, CNT/ITO IE, and AgNWs/CNT/ITO IE treated with the same concentration of bacteria by NMF-TENG electric stimulation in single AgNWs, as shown in Figure S12. The results showed that AgNWs/CNT/ITO IE (90%) > CNT/ITO IE (200 V) (72%) > ITO IE (200 V) (50%) > AgNWs (200 V) (41%) > AgNWs (10%). Therefore, the alternating current output by the NMF-TENG at a low-frequency signal of 1 Hz could generate a locally enhanced electric field close to 1 MV m^{-1} between the interdigital electrodes of the AgNWs/CNT nanowires (Figure S13), which played a role in the electrical breakdown and bacterial killing.

On the other hand, the high-voltage electric field generated by the flexible AgNWs/CNT/ITO nanosheets could promote the AgNWs to release Ag^+ and promote Ag^+ to be tightly adsorbed to the cell membrane and to react with cell wall peptidoglycan, destruction of inherent components of bacteria or production dysfunction, to achieve sterilizing effects (Figure 5c). *E. coli* thin-film samples containing ~10^6 CFU mL^{-1} bacteria were prepared to test further the bactericidal effect of the wearable self-propelled sterilization device. The sterilizing NMF-TENG device was then attached to the film, processed at different times, and grown on an AGAR plate overnight for colony observation. Colony counts calculated bactericidal efficacy at different time points. These findings (Figure 5d)

https://doi.org/10.1021/acsaelm.3c00262
ACS Appl. Electron. Mater. 2023, 5, 2819−2828

showed that the number of colonies in the AGAR medium visually decreased as the sterilization time was extended. Quantitative calculations of bacterial removal efficiency are shown in Figure 5f. As the sterilization device processing time increased, the sterilization efficiency increased significantly. 90% of *E. coli* was effectively killed after continuous treatment for 25 min, proving that the modification device has good sterilizing performance.

4. CONCLUSIONS

Briefly, a high-performance, robust, and flexible positive-friction PA66/EC nanofiber composite film was prepared by the two-component electrospinning process by controlling the ratio of the two components. Due to the high specific surface area formed by the porous electrospinning nanofiber membrane and the high electron supply ethoxy group brought by EC, the frictional contact area of NMF-TENG could be effectively increased, and a higher surface charge density was induced. The NMF-TENG produced a high output of 302 V and 0.4 μA under a low-frequency motion of 1 Hz, ensuring strong power supply for the wearable-sterilizing device. Then, the patterned AgNWs/CNT/ITO nanowire interdigital electrode was prepared by simple spin coating and direct laser writing, which had good flexibility and high conductivity and could attach perfectly to the surface of the human body. Using NMF-TENG to drive AgNWs/CNT/ITO nanowire interdigitate electrode, a wearable, self-powered, long-acting germicide device was fabricated, allowing disinfecting ions of bacteria and viruses growing in the body. This device used the tip effect, caused by nanowires, to generate a local sustained electric field of 1 MV m^{-1}, which can destroy the external structure of microorganisms and promote AgNWs to release Ag^+ (antibacterial ions). The high-voltage sterilization and the antibacterial ions' synergistic working principle largely promote the efficiency and lifetime of the antibacterial system. This self-powered sterilization system with sterilization methods has a sterilization rate of up to 90% after 25 min of low-frequency signal operation, which demonstrates enormous potential for applications in the sterilization of wearable electronics.

■ ASSOCIATED CONTENT

Supporting Information

The Supporting Information is available free of charge at https://pubs.acs.org/doi/10.1021/acsaelm.3c00262.

SEM images of PA66/EC films with different mass ratios; output power density of NMF-TENG under 3.5 Hz impact; electrode gap size distribution; electrode width size distribution; diameter distribution of AgNWs/CNT nanowires; physical picture of AgNWs/CNT/ITO nanowire interdigital electrode; physical picture of wearable self-powered sterilization device; and intensity of electric field generated by AgNWs/CNT/ITO nanowires interdigital electrode stimulated by the output voltage of NMF-TENG at 1 Hz (PDF)

■ AUTHOR INFORMATION

Corresponding Authors

Caofeng Pan − *Beijing Institute of Nanoenergy and Nanosystems, Chinese Academy of Sciences, Beijing 101400, China;* orcid.org/0000-0001-6327-9692; Email: cfpan@binn.cas.cn

Hongzhi Cui − *College of Materials Science and Engineering, Ocean University of China, Qingdao 266100, China;* Email: cuihongzhi@ouc.edu.cn

Xiaoyi Li − *College of Materials Science and Engineering, Ocean University of China, Qingdao 266100, China; Key Lab for Special Functional Materials of Ministry of Education, School of Materials Science and Engineering, Henan University, Kaifeng 475004, China;* orcid.org/0000-0001-5082-6757; Email: lixiaoyi@ouc.edu.cn

Authors

Danni Lei − *College of Materials Science and Engineering, Ocean University of China, Qingdao 266100, China*

Junpeng Wu − *College of Materials Science and Engineering, Ocean University of China, Qingdao 266100, China*

Yunlong Zi − *Hong Kong University of Science and Technology, Guangzhou 510000, China*

Complete contact information is available at: https://pubs.acs.org/10.1021/acsaelm.3c00262

Author Contributions

⊥D.L. and J.W. contributed equally to this work. D.L.: data curation, formal analysis, investigation, validation, writing—original draft. J.W.: data curation, formal analysis, investigation, validation, writing—original draft. C.P. and Y.Z.: resources, supervision. H.C.: resources, supervision. X.L.: conceptualization, resources, funding acquisition, supervision, writing—review & editing.

Notes

The authors declare no competing financial interest.

■ ACKNOWLEDGMENTS

The research was supported by the Open Project of Key Lab of Special Functional Materials of Ministry of Education, Henan University (KFKT-2022-11), the National Natural Science Foundation of China (no. 52101390), the Natural Science Foundation of Shandong Province, China (no. ZR2021QE043), and the Fundamental Research Funds for the Central Universities, China (grant no. 202112011).

■ REFERENCES

(1) Wu, K.; Tang, X.; An, E. J.; Yun, Y. H.; Kim, S.-J.; Moon, H. C.; Kong, H.; Kim, S. H.; Jeong, Y. J. Screen Printing of Graphene-Based Nanocomposite Inks for Flexible Organic Integrated Circuits. *Org. Electron.* **2022**, *108*, No. 106603.

(2) Li, Di.; Wang, C.; Cui, X.; Chen, D.; Fei, C.; Yang, Y. Recent Progress and Development of Interface Integrated Circuits for Piezoelectric Energy Harvesting. *Nano Energy* **2022**, *94*, No. 106938.

(3) Dai, Y.; Hu, H.; Wang, M.; Xu, J.; Wang, S. Stretchable Transistors and Functional Circuits for Human-Integrated Electronics. *Nat. Electron.* **2021**, *4*, 17−29.

(4) Parbrook, P. J.; Corbett, B.; Han, J.; Seong, T.; Amano, H. Micro-Light Emitting Diode: From Chips to Applications. *Laser Photonics Rev.* **2021**, *15*, No. 2000133.

(5) Zhu, Q.-B.; Li, B.; Yang, D.-D.; Liu, C.; Feng, S.; Chen, M.-L.; Sun, Y.; Tian, Y.-N.; Su, X.; Wang, X.-M.; Qiu, S.; Li, Q.-W.; Li, X.-M.; Zeng, H.-B.; Cheng, H.-M.; Sun, D.-M. A Flexible Ultrasensitive Optoelectronic Sensor Array for Neuromorphic Vision Systems. *Nat. Commun.* **2021**, *12*, No. 1798.

(6) Joo, H.; Lee, Y.; Kim, J.; Yoo, J.-S.; Yoo, S.; Kim, S.; Arya, A. K.; Kim, S.; Choi, S. H.; Lu, N.; Lee, H. S.; Kim, S.; Lee, S.-T.; Kim, D.-H. Soft Implantable Drug Delivery Device Integrated Wirelessly with Wearable Devices to Treat Fatal Seizures. *Sci. Adv.* **2021**, *7*, No. eabd4639.

(7) Jia, Y.; Jiang, Q.; Sun, H.; Liu, P.; Hu, D.; Pei, Y.; Liu, W.; Crispin, X.; Fabiano, S.; Ma, Y.; Cao, Y. Wearable Thermoelectric Materials and Devices for Self-Powered Electronic Systems. *Adv. Mater.* **2021**, *33*, No. 2102990.
(8) Peng, X.; Dong, K.; Ye, C.; Jiang, Y.; Zhai, S.; Cheng, R.; Liu, D.; Gao, X.; Wang, J.; Wang, Z. L. A Breathable, Biodegradable, Antibacterial, and Self-Powered Electronic Skin Based on All-Nanofiber Triboelectric Nanogenerators. *Sci. Adv.* **2020**, *6*, No. eaba9624.
(9) Zhang, W.; Zhang, Y.; Yang, G.; Hao, X.; Lv, X.; Wu, F.; Liu, J.; Zhang, Y. Wearable and Self-Powered Sensors Made by Triboelectric Nanogenerators Assembled from Antibacterial Bromobutyl Rubber. *Nano Energy* **2021**, *82*, No. 105769.
(10) Gao, Y.-N.; Wang, Y.; Yue, T.-N.; Weng, Y.-X.; Wang, M. Multifunctional Cotton Non-Woven Fabrics Coated with Silver Nanoparticles and Polymers for Antibacterial, Superhydrophobic and High Performance Microwave Shielding. *J. Colloid Interface Sci.* **2021**, *582*, 112−123.
(11) Feng, H.; Li, H.; Xu, J.; Yin, Y.; Cao, J.; Yu, R.; Wang, B.; Li, R.; Zhu, G. Triboelectric Nanogenerator Based on Direct Image Lithography and Surface Fluorination for Biomechanical Energy Harvesting and Self-Powered Sterilization. *Nano Energy* **2022**, *98*, No. 107279.
(12) Liu, W.; Sun, Y.; Cui, A.; Xia, Y.; Yan, Q.; Song, Y.; Wang, L.; Shan, G.; Wang, X. Electrothermal Sterilization and Self-Powered Real-Time Respiratory Monitoring of Reusable Mask Based on Ag Micro-Mesh Films. *Nano Energy* **2023**, *105*, No. 107987.
(13) Alizadeh, S.; Farshi, P.; Farahmandian, N.; Ahovan, Z. A.; Hashemi, A.; Majidi, M.; Azadbakht, A.; Darestanifarahani, M.; Sepehr, K. S.; Kundu, S. C.; Gholipourmalekabadi, M. Synergetic Dual Antibiotics-Loaded Chitosan/Poly (Vinyl Alcohol) Nanofibers with Sustained Antibacterial Delivery for Treatment of XDR Bacteria-Infected Wounds. *Int. J. Biol. Macromol.* **2023**, *229*, 22−34.
(14) Zhang, Y.; Wang, M.; Kang, S.; Pan, T.; Deng, H.; Shan, W.; He, H. Investigation of Suitable Precursors for Manganese Oxide Catalysts in Ethyl Acetate Oxidation. *J. Environ. Sci.* **2021**, *104*, 17−26.
(15) Kotnik, T.; Frey, W.; Sack, M.; Meglič, S. H.; Peterka, M.; Miklavčič, D. Electroporation-Based Applications in Biotechnology. *Trends Biotechnol.* **2015**, *33*, 480−488.
(16) Wang, D.; Zhu, B.; He, X.; Zhu, Z.; Hutchins, G.; Xu, P.; Wang, W.-N. Iron Oxide Nanowire-Based Filter for Inactivation of Airborne Bacteria. *Environ. Sci.: Nano* **2018**, *5*, 1096−1106.
(17) Huo, Z.-Y.; Du, Y.; Chen, Z.; Wu, Y.-H.; Hu, H.-Y. Evaluation and Prospects of Nanomaterial-Enabled Innovative Processes and Devices for Water Disinfection: A State-of-the-Art Review. *Water Res.* **2020**, *173*, No. 115581.
(18) Liu, C.; Xie, X.; Zhao, W.; Liu, N.; Maraccini, P. A.; Sassoubre, L. M.; Boehm, A. B.; Cui, Y. Conducting Nanosponge Electroporation for Affordable and High-Efficiency Disinfection of Bacteria and Viruses in Water. *Nano Lett.* **2013**, *13*, 4288−4293.
(19) Tian, J.; Feng, H.; Yan, L.; Yu, M.; Ouyang, H.; Li, H.; Jiang, W.; Jin, Y.; Zhu, G.; Li, Z.; Wang, Z. L. A Self-Powered Sterilization System with Both Instant and Sustainable Anti-Bacterial Ability. *Nano Energy* **2017**, *36*, 241−249.
(20) Huo, Z.-Y.; Kim, Y.-J.; Suh, I.-Y.; Lee, D.-M.; Lee, J. H.; Du, Y.; Wang, S.; Yoon, H.-J.; Kim, S.-W. Triboelectrification Induced Self-Powered Microbial Disinfection Using Nanowire-Enhanced Localized Electric Field. *Nat. Commun.* **2021**, *12*, No. 3693.
(21) Li, C.; Guo, H.; Wu, Z.; Wang, P.; Zhang, D.; Sun, Y. Self-Healable Triboelectric Nanogenerators: Marriage between Self-Healing Polymer Chemistry and Triboelectric Devices. *Adv. Funct. Mater.* **2023**, *33*, No. 2208372.
(22) Li, X.; Tao, J.; Zhu, J.; Pan, C. A Nanowire Based Triboelectric Nanogenerator for Harvesting Water Wave Energy and Its Applications. *APL Mater.* **2017**, *5*, No. 074104.
(23) Li, X.; Xu, G.; Xia, X.; Fu, J.; Huang, L.; Zi, Y. Standardization of Triboelectric Nanogenerators: Progress and Perspectives. *Nano Energy* **2019**, *56*, 40−55.
(24) Wang, C.; Wang, P.; Chen, J.; Zhu, L.; Zhang, D.; Wan, Y.; Ai, S. Self-Powered Biosensing System Driven by Triboelectric Nanogenerator for Specific Detection of Gram-Positive Bacteria. *Nano Energy* **2022**, *93*, No. 106828.
(25) Chen, J.; Wang, P.; Li, J.; Wang, C.; Wang, J.; Zhang, D.; Peng, Y.; Wang, B.; Wu, Z. Self-Powered Antifouling UVC Pipeline Sterilizer Driven by the Discharge Stimuli Based on the Modified Freestanding Rotary Triboelectric Nanogenerator. *Nano Energy* **2022**, *95*, No. 106969.
(26) Zhou, Z.; Wang, P.; Li, J.; Wang, C.; Chen, J.; Zhu, L.; Zhu, H.; Zhang, D. A Self-Powered Microbiosensor System for Specific Bacteria Detection Based on Triboelectric Nanogenerator. *Nano Energy* **2022**, *98*, No. 107317.
(27) Sun, X.; Feng, Y.; Wang, B.; Liu, Y.; Wu, Z.; Yang, D.; Zheng, Y.; Peng, J.; Feng, M.; Wang, D. A New Method for the Electrostatic Manipulation of Droplet Movement by Triboelectric Nanogenerator. *Nano Energy* **2021**, *86*, No. 106115.
(28) Liu, J.; Wen, Z.; Lei, H.; Gao, Z.; Sun, X. A Liquid−Solid Interface-Based Triboelectric Tactile Sensor with Ultrahigh Sensitivity of 21.48 KPa−1. *Nano-Micro Lett.* **2022**, *14*, No. 88.
(29) Chen, C.; Wen, Z.; Shi, J.; Jian, X.; Li, P.; Yeow, J. T. W.; Sun, X. Micro Triboelectric Ultrasonic Device for Acoustic Energy Transfer and Signal Communication. *Nat. Commun.* **2020**, *11*, No. 4143.
(30) Chen, J.; Wei, X.; Wang, B.; Li, R.; Sun, Y.; Peng, Y.; Wu, Z.; Wang, P.; Wang, Z. L. Design Optimization of Soft-Contact Freestanding Rotary Triboelectric Nanogenerator for High-Output Performance. *Adv. Energy Mater.* **2021**, *11*, No. 2102106.
(31) Wang, P.; Zhang, S.; Zhang, L.; Wang, L.; Xue, H.; Wang, Z. L. Non-Contact and Liquid−Liquid Interfacing Triboelectric Nanogenerator for Self-Powered Water/Liquid Level Sensing. *Nano Energy* **2020**, *72*, No. 104703.
(32) Li, X.; Lau, T. H.; Guan, D.; Zi, Y. A Universal Method for Quantitative Analysis of Triboelectric Nanogenerators. *J. Mater. Chem. A* **2019**, *7*, 19485−19494.
(33) Li, X.; Liang, R.; Tao, J.; Peng, Z.; Xu, Q.; Han, X.; Wang, X.; Wang, C.; Zhu, J.; Pan, C.; Wang, Z. L. Flexible Light Emission Diode Arrays Made of Transferred Si Microwires-ZnO Nanofilm with Piezo-Phototronic Effect Enhanced Lighting. *ACS Nano* **2017**, *11*, 3883−3889.
(34) Wu, Z.; Wang, P.; Zhang, B.; Guo, H.; Chen, C.; Lin, Z.; Cao, X.; Wang, Z. L. Highly Durable and Easily Integrable Triboelectric Foam for Active Sensing and Energy Harvesting Applications. *Adv. Mater. Technol.* **2021**, *6*, No. 2000737.
(35) Xu, S.; Feng, Y.; Liu, Y.; Wu, Z.; Zhang, Z.; Feng, M.; Zhang, S.; Sun, G.; Wang, D. Gas-Solid Two-Phase Flow-Driven Triboelectric Nanogenerator for Wind-Sand Energy Harvesting and Self-Powered Monitoring Sensor. *Nano Energy* **2021**, *85*, No. 106023.
(36) Li, X.; Tao, J.; Wang, X.; Zhu, J.; Pan, C.; Wang, Z. L. Networks of High Performance Triboelectric Nanogenerators Based on Liquid−Solid Interface Contact Electrification for Harvesting Low-Frequency Blue Energy. *Adv. Energy Mater.* **2018**, *8*, No. 1800705.
(37) Zheng, Y.; Liu, T.; Wu, J.; Xu, T.; Wang, X.; Han, X.; Cui, H.; Xu, X.; Pan, C.; Li, X. Energy Conversion Analysis of Multilayered Triboelectric Nanogenerators for Synergistic Rain and Solar Energy Harvesting. *Adv. Mater.* **2022**, *34*, No. 2202238.
(38) Xu, G.; Li, X.; Xia, X.; Fu, J.; Ding, W.; Zi, Y. On the Force and Energy Conversion in Triboelectric Nanogenerators. *Nano Energy* **2019**, *59*, 154−161.
(39) Jiang, J.; Sun, X.; Wen, Z. Perspectives of Triboelectric Sensors for Internet of Healthcare. *Adv. Sens. Res.* **2022**, *1*, No. 2200011.
(40) Chen, Y.; Gao, Z.; Zhang, F.; Wen, Z.; Sun, X. Recent Progress in Self-powered Multifunctional E-skin for Advanced Applications. *Exploration* **2022**, *2*, No. 20210112.
(41) Fan, F.-R.; Tian, Z.-Q.; Wang, Z. L. Flexible Triboelectric Generator. *Nano Energy* **2012**, *1*, 328−334.
(42) Wang, X.; Yang, B.; Liu, J.; Zhu, Y.; Yang, C.; He, Q. A Flexible Triboelectric-Piezoelectric Hybrid Nanogenerator Based on P(VDF-

https://doi.org/10.1021/acsaelm.3c00262
ACS Appl. Electron. Mater. 2023, 5, 2819−2828

TrFE) Nanofibers and PDMS/MWCNT for Wearable Devices. *Sci. Rep.* **2016**, *6*, No. 36409.
(43) Li, H.; Fang, X.; Li, R.; Liu, B.; Tang, H.; Ding, X.; Xie, Y.; Zhou, R.; Zhou, G.; Tang, Y. All-Printed Soft Triboelectric Nanogenerator for Energy Harvesting and Tactile Sensing. *Nano Energy* **2020**, *78*, No. 105288.
(44) Qiu, Y.; Fang, H.; Guo, J.; Wu, H. Fully Nano/Micro-Fibrous Triboelectric on-Skin Patch with High Breathability and Hydrophobicity for Physiological Status Monitoring. *Nano Energy* **2022**, *98*, No. 107311.
(45) Fan, C.; Huang, J.; Mensah, A.; Long, Z.; Sun, J.; Wei, Q. A High-Performance and Biodegradable Tribopositive Poly-ε-Caprolactone/Ethyl Cellulose Material. *Cell Rep. Phys. Sci.* **2022**, *3*, No. 101012.
(46) Uchida, S.; Houjo, M.; Tochikubo, F. Efficient Sterilization of Bacteria by Pulse Electric Field in Micro-Gap. *J. Electrost.* **2008**, *66*, 427−431.
(47) Zhang, X.; Huang, H.; Zhang, W.; Hu, Z.; Li, X.; Liu, J.; Xu, G.; Yang, C. Self-Powered Triboelectric Nanogenerator Driven Nanowires Electrode Array System for the Urine Sterilization. *Nano Energy* **2022**, *96*, No. 107111.
(48) Yao, G.; Jiang, D.; Li, J.; Kang, L.; Chen, S.; Long, Y.; Wang, Y.; Huang, P.; Lin, Y.; Cai, W.; Wang, X. Self-Activated Electrical Stimulation for Effective Hair Regeneration *via* a Wearable Omnidirectional Pulse Generator. *ACS Nano* **2019**, *13*, 12345−12356.
(49) Yuan, R.; Yang, N.; Fan, S.; Huang, Y.; You, D.; Wang, J.; Zhang, Q.; Chu, C.; Chen, Z.; Liu, L.; Ge, L. Biomechanical Motion-Activated Endogenous Wound Healing through LBL Self-Powered Nanocomposite Repairer with PH-Responsive Anti-Inflammatory Effect. *Small* **2021**, *17*, No. 2103997.

https://doi.org/10.1021/acsaelm.3c00262
ACS Appl. Electron. Mater. 2023, 5, 2819−2828